ELSEVIER

Journal of Atmospheric and Solar-Terrestrial Physics 68 (2006) 102–113

Journal of ATMOSPHERIC AND SOLAR-TERRESTRIAL PHYSICS

www.elsevier.com/locate/jastp

Statistics of sporadic iron layers and relation to atmospheric dynamics

Jan C. Diettrich[a,*], Graeme J. Nott[a], Patrick J. Espy[a], Xinzhao Chu[b], Dennis Riggin[c]

[a]*Physical Science Division, British Antarctic Survey, Cambridge, CB4 0ET, UK*
[b]*University of Illinois, Urbana, IL, USA*
[c]*Colorado Research Associates, Boulder, CO, USA*

Available online 26 September 2005

Abstract

At Rothera Research Station (67.3°S, 68.1°W), Antarctica, 296 h of day and nighttime Fe-Boltzmann temperature lidar data were accumulated in 2003. During this time, sporadic iron layers (Fe_S) were observed with an annual average occurrence probability of 14%. The peak altitude of the Fe_S layers was highest during the summer, with a fitted value of 103 km while during the winter the layer decreased in height to 90 km with an annual average of 97 km. The atmospheric temperature perturbations and potential energy density profiles computed from the same lidar data exhibited increased temperature but constant-with-height potential energy density when sporadic Fe layer occurred. Once sporadic Fe layers disappeared, the potential energy density decreased with height, indicating an energy loss due to atmospheric gravity wave breaking. These results suggest a link between Fe_S and atmospheric dynamics.

Keywords: Antarctic; Lidar; Sporadic iron layer

1. Introduction

The formation of sporadic metal layers has been of interest since their discovery, see Kirchhoff and Clemesha (1973) or Clemesha et al. (1978) for early reports. Sporadic sodium layers (Na_S) in the mesosphere have been linked to temperature (Gardner et al., 1991), sporadic E layers (Beatty et al., 1989; Nagasawa and Abo, 1995), indirectly to auroral precipitation (von Zahn et al., 1987), and to atmospheric gravity wave activity (Gardner et al., 1995). Hansen and von Zahn (1990) suggested that a combination of these mechanisms are responsible for the generation of Na_S, while Friedman et al. (2000) discussed different generation mechanisms for different altitude ranges. Cox and Plane (1998) have shown that Na_S may be formed within minutes when sporadic E layers descend to about 90 km, with the sporadic E layers most likely being generated by wind shears associated with tidal or gravity-wave forcing.

Sporadic iron layers (Fe_S), first reported by Granier et al., (1989), are less understood than Na_S due to a dearth of data. A multi-instrument campaign gave some insight into the combined appearance pattern of sporadic E layers, Fe^+, and

*Corresponding author. Tel.: +44 1223 221549; fax.: +44 1223 221226.
E-mail address: jadi@bas.ac.uk (J.C. Diettrich).

1364-6826/$ - see front matter © 2005 Elsevier Ltd. All rights reserved.
doi:10.1016/j.jastp.2005.08.008

sporadic Fe layers (Alpers et al., 1993). By combining the lidar observations of sporadic Fe layers from the German Polarstern voyage in the low and middle southern latitudes with northern polar latitude at Andøya (69°N), Alpers et al. (1994) reported the dependence of occurrence probability, altitude and width of Fe_S on latitude. Kane and Gardner (1993) linked the Fe_S to sporadic E layers and investigated the influence of chemistry on Fe_S formation. However, all these observations were limited to nighttime only. Plane et al. (2003b) demonstrated that an Fe_S layer may result from a descending sporadic E layer that contains Fe^+. The height of the Fe_S formation is then related to the ratio of oxygen atoms to free electrons. Here, by understanding the formation processes of Fe_S, and sporadic metal layers in general, a great deal can be learned about atmospheric chemistry, reservoirs of iron and other metals, and dynamic processes occurring in the mesosphere and lower thermosphere. Data covering full diurnal cycle throughout a year are essential for a clear understanding to fully model Fe_S.

In this paper, we report on about 42 h of sporadic iron layer data from a total of 296 h of observations covering full diurnal cycles at Rothera (67.3°S, 68.1°W), Antarctica, during 2003. The mean altitude of the Fe_S was found to vary with season and this will be discussed in the initial part of this paper along with the annual and daily occurrence frequency of the sporadic layers. In the second part the relationship between the Fe_S and atmospheric dynamics, particularly temperature enhancement and potential energy, will be investigated.

2. Experiment and data analysis

As part of the collaboration between the University of Illinois and the British Antarctic Survey, an Fe-Boltzmann temperature lidar was deployed at Rothera in December 2002. The dual-laser system, operating at 372 and 374 nm, probes a ground state and a low-lying excited state of mesospheric atomic iron. Iron density may be derived from the ground state 372 nm alone. However, as the energy separation to the excited state is small, the state populations are in thermal equilibrium (Pendleton et al., 1993), and the temperature may be derived from the ratio of the 374–372 nm return signal using the Boltzmann relation. Although solar scatter in the UV is severe, the lidar operates in a Frauenhoffer line that allows for both day and night operation. Thus, it provides Fe data with full diurnal coverage.

The system has been described in detail by Chu et al. (2002) and only salient points regarding its operation will be presented here. Each individual photon count profile was integrated for 2.5 min, and the system was gated to obtain 48 m height resolution. Each profile was smoothed vertically with a Hamming window with a full-width at half-maximum (FWHM) of 2500 m. For each Fe density profile a Gaussian profile was fitted to the smoothed normal iron layer. The Gaussian fit was then subtracted from the smoothed data and the residual was calculated. A second Gaussian fit was applied to the residual if an additional iron peak (Fe_S) was present. These Gaussian fits quantified Fe and Fe_S layer width, centroid height and peak density with respect to time. A sample of Fe and Fe_S profile is illustrated in Fig. 1, in its raw form (left subplot, thin solid line), its smoothed form (left subplot, dashed line), and the Gaussian fits to the Fe (right subplot, diamonds) and Fe_S layer (right subplot, circles, with the dashed line showing the same smoothed profile as in the left subplot). The first sporadic iron layer was observed on 1 January, 2003 at 04:52 UT. The last Fe_S layer of 2003 was observed at 09:30 UT on 29 December.

The following set of criteria were used for identifying Fe_S, where ρ denotes iron density:

(a) mean $\rho(Fe_S) >$ uncertainty of ρ(Fe at the peak),
(b) maximum of $\rho(Fe_S) > 2$ times of uncertainty of $\rho(Fe_S)$, and $\rho(Fe_S) > 500$ Fe_S/cm^3,
(c) maximum of $\rho(Fe_S) > 2$ times of standard deviation of the background noise (range of 140–160 km) and
(d) width of $\rho(Fe_S) < 15$ km.

This quantitative definition of Fe_S layers is slightly different from those introduced by other groups such as Alpers et al. (1994) where the criteria of a growth rate of $\geqslant 2\%$ per minute and a FWHM of $\leqslant 5$ km were introduced. However, the restriction on growth rate by Alpers et al. would exclude several of our Fe_S observations. As several Fe_S were already present at the start of lidar operation at Rothera, growths rate could not be determined, and hence those measurements would have to be discarded. A number of cases of Fe_S were found with widths of > 5 km, hence maximum width was increased to 15 km. However, we are aware that

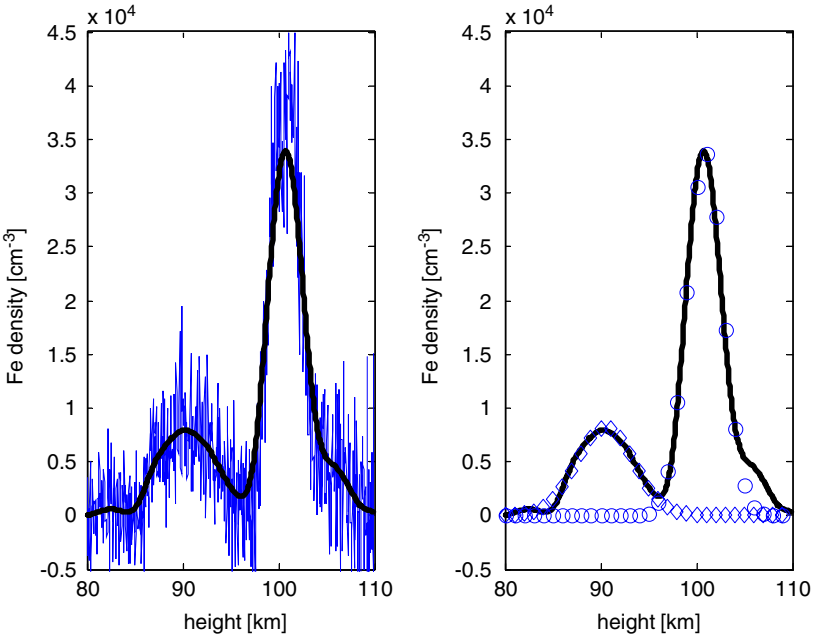

Fig. 1. Sample profile of Fe layer with sporadic Fe of a single profile taken on the 01-01-03 at 06:06 UT. Left subplot shows the raw data (solid line) with smoothed data (dashed line), and the right subplot shows the same smoothed data (dashed line) with the fitted Gaussian profiles for the common Fe layer (diamonds) and sporadic Fe layer (circles).

different criteria may lead to different statistical results.

3. Statistical observations

3.1. Fe_s statistics

The Fe-Boltzmann lidar is capable of both day and night measurements, weather permitting. Our lidar operations at Rothera were mainly limited by the local weather conditions, system maintenance, and operator availability. As it will be shown later in Fig. 3, actually more data were collected in summer than in winter since more operators were available during summer seasons. Throughout the year of 2003, Fe density data were collected in a total of 296 h on 58 different days and nights. During this period, 117 h were collected in the nighttime period (sun zenith angle $>90^\circ$), while the rest 179 h were in daylight conditions (sun zenith angle $<90^\circ$). Among the 296 h, sporadic Fe layers were observed for a total of 42.3 h and the overall occurrence probability of Fe_S was 14% at Rothera. The first sporadic iron layer was observed on first January 2003 at 04:52 UT, and the last one was at 09:30 UT on 29 December 2003. The 42.3 h of Fe_S occurred in 18 different events (day and/or night), in which 14 events were in daytime and four events were in nighttime with 34 and 8 h of Fe_S, respectively. Thus, the sporadic Fe layers at Rothera showed unequal occurrence probabilities of 19% and 7% for the daytime and nighttime, respectively. The statistics of the lidar operation and Fe_S hours are summarized in Table 1.

Histograms of the peak density, peak altitude, and FWHM of the sporadic Fe layers are plotted in Fig. 2 (layer width will be given as FWHM throughout the paper if not stated otherwise). The left panel shows the statistics for the overall daytime and nighttime Fe_S, while the right panel illustrates the nighttime only data. The peak altitude of Rothera Fe_S exhibits a large variation from the lowest at 80 km to the highest at 116 km, with two occurrence maxima around 91 and 106 km. Some sporadic Fe layers were observed within the range of normal Fe layer and were evident as large, sharp, temporarily restricted increases in iron density and fulfilled the criteria set out for the sporadic Fe layers. The Fe_S between 80 and 86 km originates from a single observation made on 23 April, 2003. The peak density varies over a large range from $\sim$5000 to $4.5\times10^4\,cm^{-3}$. The occurrence of Fe_S

Table 1
Mean characteristics of observed Fe_S at Rothera for 2003, along with comparisons to the Andøya (from Alpers et al., 1994) and Urbana (from Kane and Gardner, 1993) nighttime observations

	Rothera (67.3°S, 68.1°W)			Urbana	Andøya
	Overall (day and night)	Day only	Night only	Night only	Night only
Operation of Lidar	296 h 58 events	179 h 35 events	117 h 36 events	325 h	118.4 h
Observation of Fe_S	42.3 h 18 events	34 h 14 events	8.3 h 4 events	88 h 34 events	35 events
Occurrence probability (%)	14.3	19	7.1	27	30
Mean height Fe (km)	88.0±2.3	89.0±1.9	86.4±2.0	88.1	—
Mean width Fe (km)	8.3±2.5	7.8±2.2	9.2±2.6	3.4	—
Mean peak density Fe ($\times 10^3\,cm^{-3}$)	10.1±5.3	9.1±4.1	11.6±6.4	12.4	—
Mean height Fe_S (km)	100.6±8.0	100.9±7.9	99.4±8.0	100	90–94
Mean width Fe_S (km)	5.1±2.7	5.2±2.9	4.7±1.7	2	1–3.5
Mean peak density Fe_S ($\times 10^3\,cm^{-3}$)	10.7±10.4	10.7±10.9	10.7±7.9	10	—

Continuous operation from day into night, or from night into day, was counted as events for both day and night, hence the sum of day and night operation events is larger than the overall value for day and night.

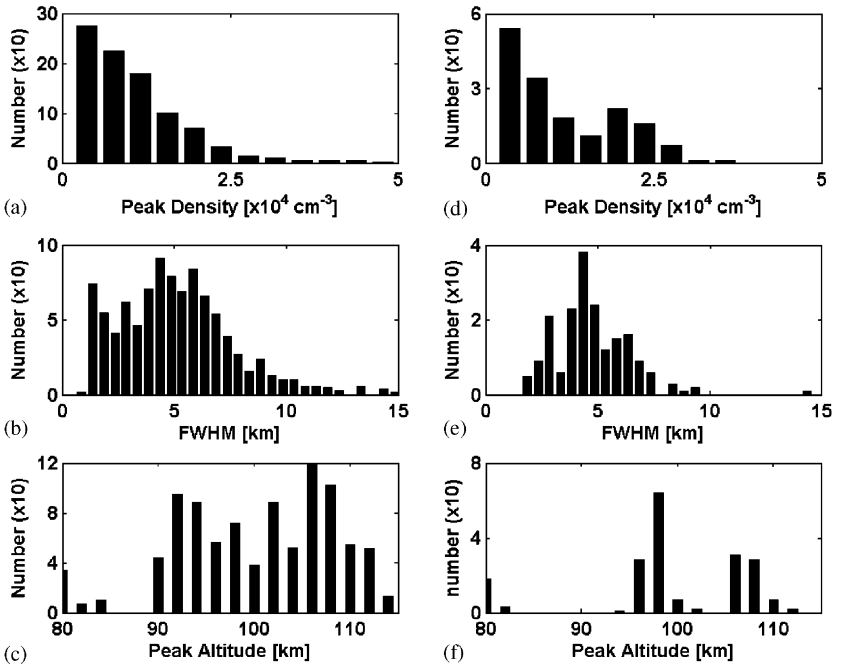

Fig. 2. Histograms of the sporadic Fe layers observed at Rothera for 2003. The left panel is for the overall day and night Fe_S, while the right panel is for the nighttime Fe_S only. Three subplots in each panel consist of the statistics of Fe_S peak density, peak altitude and width.

peak density exhibits a nearly exponential decay: the larger the density, the fewer the Fe_S event occurrences. Most of the Fe_S at Rothera have FWHM between 1 and 8 km, with some over 10 km and very few reach 15 km. Compared with the day and night statistics, Rothera nighttime only Fe_S have occurrence maximum of FWHM around 4.5 km, and relatively narrower distributions of FWHM, peak altitude and peak density. A comparison of Rothera nighttime Fe_S with nighttime observations at Andøya and Urbana will be given in a later section.

Two of several theories describing sporadic layer formation are: the sporadic layers within the body of the normal metal layers could result from

wave-induced compression; and the sporadic layers at higher altitudes are strongly correlated with ion layers, especially descending sporadic E layers (Plane et al., 2003b). Sporadic E layers are thin layers of concentrated plasma (Fe^+, Mg^+, etc. and an equal concentration of electrons) occurring in the lower thermosphere between about 90 and 120 km. Ion-induced Fe_S are usually very narrow with density significantly greater than the background layer. Rothera Fe_S above 100 km occupy ~56% of the total observations, and they are most likely the ion-induced layers since the density of normal Fe layers above 100 km is too low to form wave-induced Fe_S. However, in considerably many cases, such high-altitude Fe_S are much wider than normally claimed ion-induced layers (<2 km). This situation is clearly illustrated in Fig. 3, in which the peak altitudes of the sporadic Fe layers are plotted against corresponding layer widths. Hence, it is not clear whether these high-altitude Fe_S should be classified as ion-induced Fe_S. As for Fe_S between 90 and 100 km (~37% of entire Fe_S dataset), it is even more unclear which category they belong to. The Fe_S below 90 km are most likely the wave-compression-induced layers that mainly occur at the underside of the normal Fe layer with steep gradients (large mixing ratio). These layers are generally created by waves with significant amplitudes or short vertical wavelengths. Less than 6% of sporadic Fe layers were observed below 90 km at Rothera. As shown in Fig. 3, their widths are even narrower than the height altitude sporadic layers, which is contradictory to normal expectations. Currently, we have no good means or criteria to classify Rothera Fe_S into different categories. Therefore, in our statistical study here, we do not distinguish different types of Fe_S, but treat all Fe_S events in the same manner and only obtain the overall Fe_S statistics.

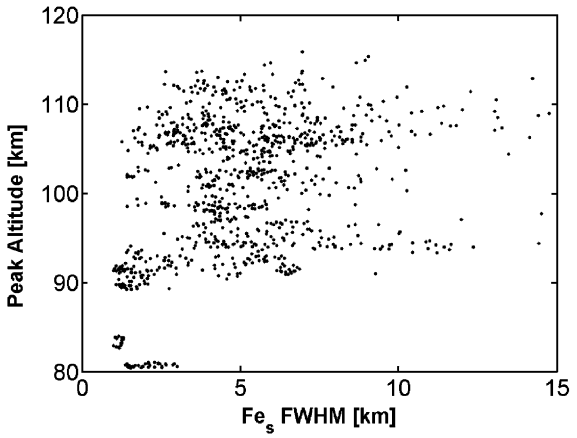

Fig. 3. Peak altitude versus FWHM of sporadic Fe layers at Rothera. Each dot represents one lidar profile of 2.5 min integration time.

The mean characteristics of Rothera sporadic Fe layers as well as normal Fe layers are summarized in Table 1 along with their statistical uncertainties. At Rothera, the annual mean width of Fe and Fe_S layers were 8.3 ± 2.5 and 5.1 ± 2.7 km, respectively. The mean height of Fe and Fe_S layers for the year was 88.0 ± 2.3 and 100.6 ± 8.0 km, respectively. The mean peak density of Fe and Fe_S layers are $10.1 \pm 5.3 \times 10^3$ and $10.7 \pm 10.4 \times 10^3$ cm^{-3}. No difference (at least not statistically significant) was observed in the mean characteristics of sporadic Fe layer height, width and peak density for the nighttime only data and the overall day and night data.

3.2. Diurnal variations

The occurrence probability of sporadic Fe layers exhibits significant diurnal variations. In contrast, there were no significant differences between daytime and nighttime mean width and mean height of the sporadic Fe layers. This can be seen in the mean values of width and height for day-only and night-only data listed in Table 1. However, the occurrence probability is much higher during the day than in the night. To investigate the diurnal variation of Fe_S occurrence probability (OP), the data were averaged in local time to obtain 48 of half-hour means. The resulting occurrence probabilities are plotted as open circles against local time in the top panel of Fig. 4, and corresponding lidar operation hours for each bin are plotted in the bottom panel of Fig. 4. Each half-hour bin contains at least 2 h of lidar data. In some cases (mainly around midnight) more than 10 h of lidar data were recorded for each bin. Strong diurnal and semidiurnal variations, with maxima at 02:00 and 15:00 LT, are clearly shown in Fig. 4.

To characterize these diurnal and semidiurnal variations, we applied a diurnal plus semi-diurnal harmonic fit to the occurrence probability using

$$f(t) = A_0 + A_{24}\cos\left\{\frac{2\pi}{24}(t-\Phi_{24})\right\} + A_{12}\cos\left\{\frac{2\pi}{12}(t-\Phi_{12})\right\}. \quad (1)$$

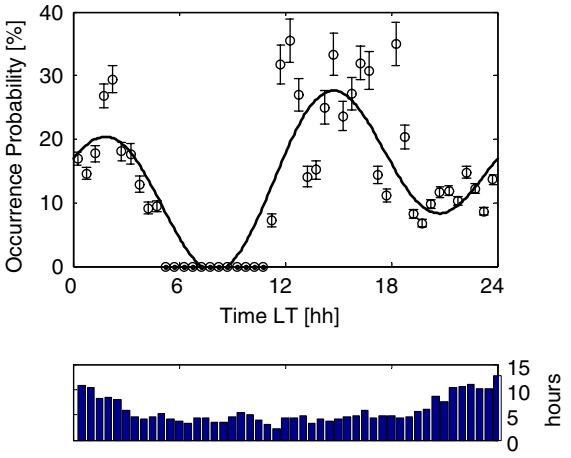

Fig. 4. Diurnal variations of sporadic Fe layers at Rothera in 2003. Plotted in the top panel is the occurrence probability of Fe_S versus local time. Data are binned in every half hour. The dashed line is a diurnal plus semi-diurnal harmonic fit to the data using Eq. (2). The bottom panel shows the histogram of lidar operation hours versus local time.

A_0 is the background OP, A_{12} and A_{24} are the amplitudes of the 12 and 24 h OP oscillations, respectively, and will be referred to as "OP amplitudes" in this section. Φ_{12} and Φ_{24} are the corresponding phases for the 12- and 24-h periods of the OP. These fitting parameters are given in Table 2. The OP amplitude of the 12-h wave has a larger value (11%) compared to the value of the 24-h wave (7%). The OP amplitude ratio of 11:7 for the 12:24-h waves suggests to agree with the ratio of 15:7 calculated with the global scale wave model (GSWM-02) (Hagan and Forbes, 2003), which supplies semidiurnal and diurnal amplitudes of the zonal winds.

An interesting feature of Fig. 4 is that no Fe_S were observed between 05:00 and 11:00 LT for the entire year in 2003, leading to the lower overall occurrence probability. One possible explanation may be the significant inter-annual variation in the occurrence probability. Another possibility is that the apparent 'hole' is due to the interplay of the 24- and 12-h waves or different 12 h tidal modes.

3.3. Seasonal variations

The peak altitude and occurrence probability of sporadic Fe layers exhibit large seasonal variations at Rothera (as shown in Fig. 5), while no trend was found in the Fe_S width. Plotted in the top panel of Fig. 5 are the mean peak heights of Fe (squares) and

Table 2
Parameters of diurnal and semidiurnal fits to the occurrence probability of Fe_S. A_0 is the mean probability, A_{24} and A_{12} are the amplitudes of the diurnal and semidiurnal variations, Φ_{24} and Φ_{12} are the phases of the diurnal and semidiurnal variations

	Fe_S OP
A_0	15.0 ± 0.01
A_{24}	7.4 ± 0.1
Φ_{24}	1140 min
A_{12}	11.2 ± 0.1
Φ_{12}	-135 min
Correlation	83%
Mean residual	4.5%

Also given are also the correlation coefficients of data points with fitted curves and their mean residual. Uncertainties of fitting values are the standard deviation of each particular parameter in the fit.

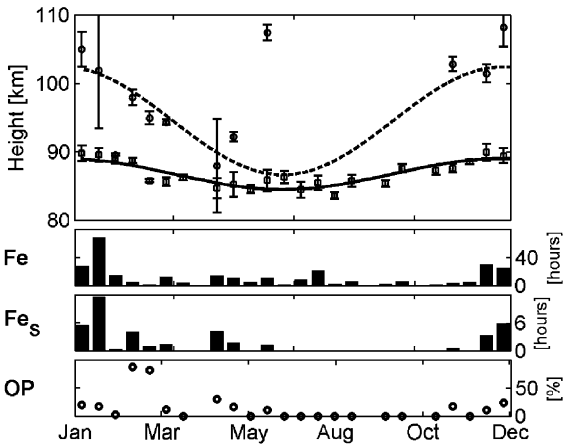

Fig. 5. Annual variations of sporadic Fe layers for 2003. Top panel presents the mean centroid height of Fe layer (squares) and sporadic Fe layer (o) for every 14 days throughout the year. The solid line is an annual harmonic fit to the Fe layer height, which contains a sinusoidal wave with period of 365 days, and the dashed line is the corresponding fit to the sporadic Fe layer height. The two middle panels show the histograms of corresponding observations hours for the Fe layer and for the Fe_S layer. The bottom panel illustrates the occurrence probability (OP) of Fe_S.

Fe_S (circles) for every 14 days throughout the year of 2003. The error bars spanning data points represent the geophysical variability of Fe or Fe_S in each 14-day period, which are computed as the standard deviation of all sample heights within each period. Except one outlier in May, the overall Fe_S altitudes showed a seasonal trend as they reached the maximum in summer (December–January) and the minimum in winter. The altitude variation is nearly 15 km for Fe_S throughout the year.

To characterize the seasonal variation, we will apply an annual fit to the Fe_S data. However, the large gap of the Fe_S data from July to October 2003 might introduce a large uncertainty in the fitting. To compensate this problem, we applied an annual fit to the normal Fe layer height to obtain the phase information, and then use the same phase in the annual fit to the Fe_S data. While the altitude of normal Fe layers also exhibited a seasonal variation, the difference from the maximum to the minimum is only half of the differences in the maximum and minimum of the Fe_S. We applied a least-square annual fit to the height of Fe using

$$f(t) = A_0 + A_{365}\cos\left\{\frac{2\pi}{365}(t - \Phi_{365})\right\}. \quad (2)$$

A_0 is the annual mean, A_{365} and Φ_{365} are the amplitude and phase of the annual variation. This fit result is shown as the solid curve in the top panel of Fig. 5. We also investigated a semi-annual fit superimposed to the annual variation, however, the correlation coefficient was not significantly improved. Therefore, the semi-annual variation is not shown in this paper. A similar annual fit was applied to the Fe_S height data using the same phase as for the fitted Fe height (here the outlier in May was discarded, due to is abnormal altitude). The result is plotted as a dashed curve in Fig. 5. This is the first report of annual variations of Fe_S height. The fitted height of Fe_S varies between 90 km during the winter and 103 km during the summer, with an annual amplitude A_{365} of 6.6 ± 0.5 km. The annual fitting parameters and their uncertainty are summarized in Table 3.

Annual modulation of mean height of the normal Fe layer has been linked to two phenomena: increased chemical reservoir capacity of atomic Fe during colder summer mesopause temperatures (Helmer and Plane, 1990) and uptake of atomic Fe on ice particles during the colder summer period at the bottom side of the Fe layer (Plane et al., 2003a). However, this explanation cannot be applied to the sporadic Fe layers. Temperatures above the mesopause are too warm to support the formation of ice particles and increasing temperatures decreases reservoir capacity. Possible mechanisms could be uplift during the summer months, or seasonal variations of different Fe_S formation processes in different height ranges. However, currently we do not have the means to distinguish different processes of Fe_S formation, to verify one or the other mechanism.

Two middle panels of Fig. 5 give, respectively, the number of hours of data gathered for normal Fe and sporadic Fe_S for each measurement period (14-day), while the bottom panel in Fig. 5 illustrates the occurrence probability of Fe_S through the year. As stated earlier, more lidar data were collected in the summer than in the winter. The occurrence probability appeared to be zero for some measurement periods, especially from July to early November, owing to the limited data samples in 2003. A seasonal variability of occurrence probability was observed with a maximum of 18% during the summer period (December–February), and a minimum of 2% in the winter (June–August). This is probably related to the strong seasonal variation of sporadic E layer that also peaks in summer. This seasonal change of occurrence probability at Rothera is more extreme than the summer/winter ratio of 1.5 reported by Kane and Gardner (1993). We are aware that our limited data samples in 2003 would introduce large uncertainties in the calculated occurrence probability. In addition, as summer data were mostly taken during daytime and winter data were taken during nighttime, the seasonal variation in occurrence probability could be biased by the diurnal variation in occurrence probability. Unfortunately, we were not able to disentangle seasonal variation from diurnal variation.

Table 3
Parameters of annual fit to the Fe and Fe_S layer heights

	Fe Height	Fe_S Height
A_0	86.7 ± 0.2 km	96.7 ± 0.5 km
A_{365}	2.3 ± 0.6 km	6.6 ± 0.5 km
Φ_{365}	15 days	15 days
Mean residual	2.7 km	4.2 km

A_0, the mean height of the Fe and the Fe_S, and A_{365} is the amplitude and Φ_{365} the phase of annual variations of the Fe layer and Fe_S.

3.4. Comparisons with Andøya and Urbana nighttime observations

Since the observations of sporadic Fe layers made at Andøya (Alpers et al., 1994) and at Urbana (Kane and Gardner, 1993) were only undertaken during nighttime, we will compare those to the Rothera nighttime data. Sporadic Fe layers at Andøya (69°N, 16°E) were detected between 89 and 106 km altitude with a reported mean widths of

≈2.5 km of the sporadic layers (Alpers et al., 1994). Kane and Gardner (1993) reported Fe_S altitudes between 90 and 115 km and a width of 2 km at Urbana, Illlinois (40°N, 88°W). Comparing with Andøya, the sporadic Fe layers at Rothera distribute in a much larger altitude range, extending to higher altitudes by more than 10 km and to lower altitude by more than 5 km. The width of Fe_S at Rothera also has a much larger distribution range than Andøya and Urbana. One immediate cause to the width difference is the different criteria used in identifying sporadic Fe layers. Alpers et al. (1994) limited the layers to less than 5 km, while we allowed the layers to be as wide as 15 km. However, the difference in Fe_S altitude distribution cannot be explained by the criteria difference. Several sporadic Fe layers above 106 km occurred in both summer time and winter time. Why Rothera exhibits much higher sporadic Fe layers than Andøya is still an open question, however, it might partially be governed by a suggested interhemispheric difference (Siskind et al, 2003).

The occurrence probability of Fe_S was reported as 30% and 27% for Andøya and Urbana by Alpers et al. (1994) and Kane and Gardner (1993), respectively. They are much higher than the Rothera nighttime occurrence probability of 7.1%. In addition, Alpers et al. (1994) nighttime observations were conducted during spring and fall only. Selecting the same time ranges from the Rothera data, Fe_S was observed for only 1 h, out of 20 h data collected over the same time period. This indicates that the occurrence probability of Fe_S at Rothera in 2003 is lower than that at Andøya observations made a decade ago.

4. Relation to atmospheric dynamics

To understand the influence of atmospheric gravity wave activity on the appearance/disappearance of sporadic Fe layers, we investigate temperature changes and potential energy in the process of Fe_S. We found that for a majority of observations temperature enhancement occurred during the occurrence of Fe_S and the potential-energy profile was modified by the presence of Fe_S.

4.1. Temperature enhancement

A relationship between the temperature enhancement and presence of the sporadic layer was also found. Fig. 6 (a) shows data from the 28 January, 2003, with height of Fe (black solid line) and of the Fe_S (black dashed line), while Fig. 6(b) shows the atmospheric temperature averaged between 85 and 95 km measured with the Fe lidar. Here, normal temperature profiles (vertical resolution of 480 m and time resolution of 10 min) were calculated first, followed by averaging the temperature profiles for the height range of 85–95 km. The overall background temperature profile with height followed the MSIS-00 temperature profile. The mean temperature during the period of Fe_S was 190 K, while no Fe_S was observed when the mean temperature was 150 K. Thus, there was a temperature increase of ≈40 K during the presence of sporadic Fe layers. A similar case (Fig. 7) was found during the night of 25 February 2003, when additional temperature measurements were conducted with a Bomem spectrometer, also located at Rothera (see Espy et al. (2003) for a description of the instrument). A clear increase of temperature during the period of sporadic Fe layer was found in Fig. 7 for both instruments. However, it is assumed that the temperature enhancement is driven by AGW activity, and the temperature structure depends on the vertical wavelength. This in mind different temperature perturbation at different altitudes could be generated, leading to a more complicated relation. Further, we are not able to clarify if wind shear, temperature enhancement, or a combination of those two is the cause for the generation of sporadic Fe layers. However, temperature increases

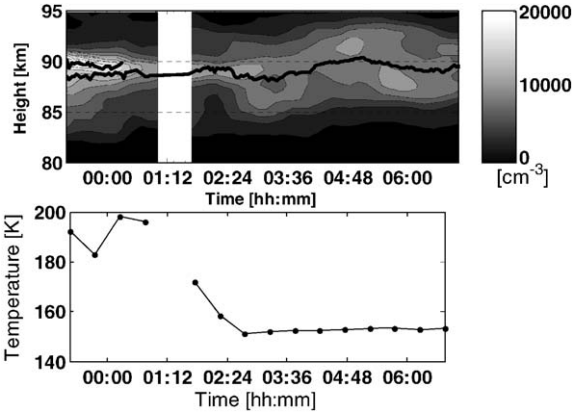

Fig. 6. (top plot) A contour plot of the iron density with calculated layer height of Fe (black line) and Fe_S (dashed black line) for the 28 January, 2003, from 23:10 to 07:25 UT. (bottom plot) The corresponding mean temperature calculated between 85 and 95 km for every half hour. See text for more explanation.

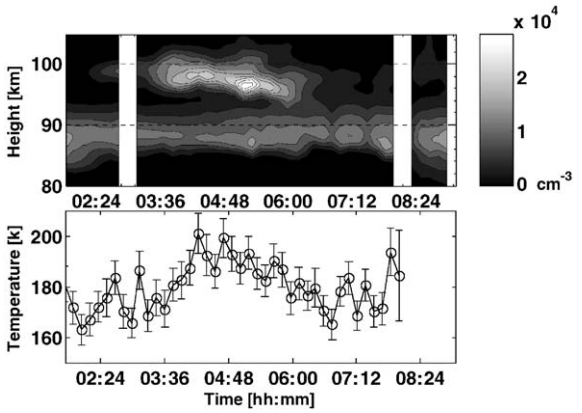

Fig. 7. (Top plot) shows a contour plot of the iron density for 25 February, 2003, from 02:30 to 07:30 UT. (bottom plot) shows the corresponding mesospheric hydroxyl temperature measured with the Bomem spectrometer located at Rothera.

during the presence of sporadic Fe layers have been observed for five out of six occasions, with an average temperature enhancement of $\approx 20 \pm 10$ K, when considering the five cases of temperature enhancement. The sixth case showed a temperature decrease of ≈ 30 K. In addition, a temperature change for the height of the sporadic layer with respect to time was also determined. Temperature changes of $\approx 0.24 \pm 0.11$ K/min were found for the time between determining maximum Fe_S layer density to the time when the sporadic layer had disappeared. An overall increase in atmospheric temperatures during the presence of sporadic layers was also reported by Qian et al. (1998) (for Na_S) and by Gardner et al. (1993) (for sporadic Fe layers).

4.2. Potential energy

The potential energy, calculated from the normalized, time-averaged temperature perturbation, T', is defined by Whiteway and Carswell (1994) as

$$E_p(z) = \frac{1}{2}\left(\frac{g}{N(z)}\right)^2 \left(\frac{T'(z)}{T_0(z)}\right)^2, \quad (3)$$

where g is the gravitational acceleration, $N(z)$ is the Brunt–Väisälä frequency profile, and $T_0(z)$ is the mean unperturbed temperature profile. As background temperature is of importance, an example will be given to explain our approach of calculating $T_0(z)$.

Fig. 8 shows a contour plot of the iron density for an observation on 10 May, 2003, between 15:30 and 23:30 UT. Superimposed are the fitted height values for the Fe and the Fe_S layer, represented by a black solid line and black dashed line, respectively.

To derive the unperturbed mean temperature, we first calculated the instant temperatures for the height ranges of: (a) iron range (75–100 km), using the Boltzmann technique (Chu et al., 2002); (b) Rayleigh range (30–57 km), using the Rayleigh technique by Hauchecorne and Chanin (1980); and (c) 0–20 km, MSIS model data (Picone et al., 2002). The height resolution was set to 480 m and measured profiles were integrated into half-hour average profiles. Resulting temperature profiles were smoothed using a Hamming window with a FWHM of 5000 m. Then the half-hour temperatures profiles were integrated through the entire observations period (15:30–23:30) to obtain one averaged temperature profile. This temperature average can smooth out most waves with periods less than 8 h. To further remove the influence of waves with large vertical wavelength, we applied a sixth order polynomial fit to this averaged temperature profile, as described by Pan and Gardner (2003), to obtain one single profile from 0 to 100 km.This single profile was then used as the unperturbed mean temperature profile $T_o(z)$. By subtracting $T_o(z)$ from each half–hour temperature profile, the temperature perturbations $T'(z)$ were determined. Potential energy can then be computed using Eq. (3).

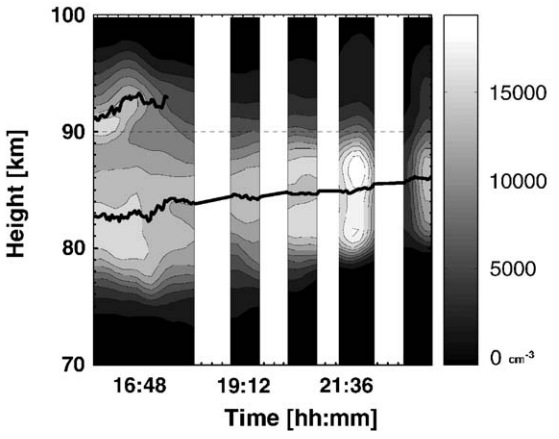

Fig. 8. Contour plot of the iron density (top) measured during 10 May, 2003 at Rothera. Superimposed on the top panel are the mean height values of the Fe layer (●) and the corresponding mean height of the sporadic iron layer (○).

Based on the criteria given earlier, Fe_S was present prior to the start of the observation period and lasted until approximately 18:30 UT. We separately calculated the potential energy of the two periods: 15:30–18:30 UT (during sporadic layer) and 19:30–23:30 UT (no sporadic layer), each being an average of six and eight half hour potential energy density profiles, respectively. The mean heights of Fe and Fe_S layers were 83.1 ± 1.0 and 91.1 ± 0.6 km, respectively, with widths of 11.4 ± 1.4 and 5.9 ± 0.7 km. Profiles of rms temperature perturbation and E_p per unit mass are shown in Fig. 9(a) and (b), respectively, with the solid line representing results for the first time period and the dashed line for the second period. The conservative growth rate, $\exp(z/2H)$ and $\exp(z/H)$ are shown for comparison in Fig. 9, as dash-dotted lines. The error propagation estimates an uncertainty in E_p per unit mass of 120 J/kg.

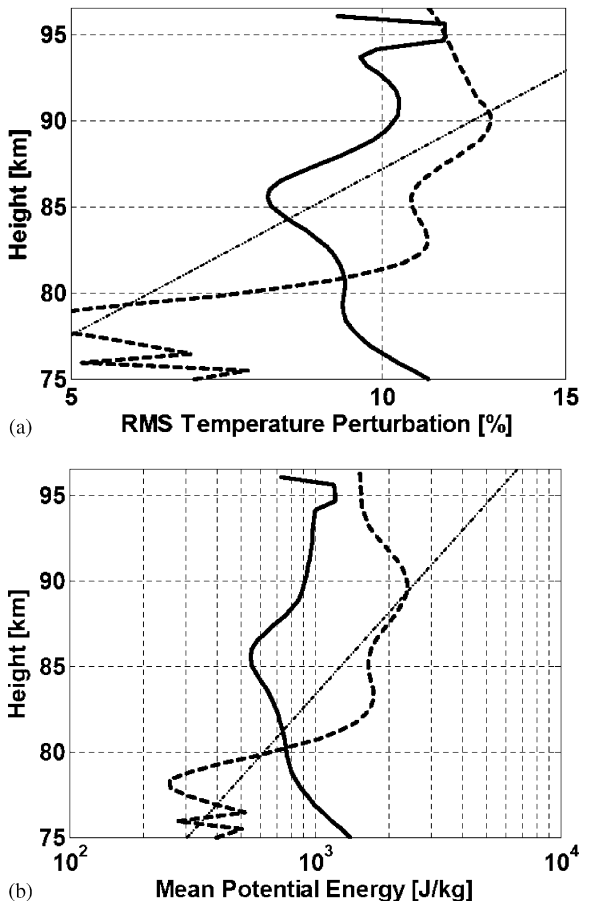

Fig. 9. Profiles for (a) rms temperature perturbation, and (b) potential energy per unit mass for data from 10 May, 2003. The dashed line shows E_P for the time period of 15:30– 18:30 UT, and the solid line for the time period of 19:30–23:20 UT. The dashed dotted lines represent the conservative growth rates: $\exp(z/2H)$ in (a) and $\exp(z/H)$ in (b).

A significant difference in the profiles can be seen for the height range of the sporadic layer. The temperature perturbation can be split roughly into two height ranges, below the sporadic layer height (75–90 km) and height range of the sporadic layer (above 90 km). When no Fe_S was detected, the temperature perturbation increased roughly without energy dissipation for the lower height range. However, a significant decrease in the temperature perturbation can be seen for the top height range. The opposite seems to be the case for the period during which the Fe_S layer was present, a large dissipation of energy below the sporadic layer and above 90 km the growth rate is close to the conservative growth rate. By looking at Fig. 9(b), where potential energy density per unit mass is given, one can see a similar pattern. Below 90 km, the wave energy increases without extreme energy dissipation, however, above 90 km a large amount of E_p is dissipated for the time period of no Fe_S presence. During the time period of Fe_S layer presence, energy is shed in the lower altitude half, whereas above 85 km, the E_p remains fairly constant, indicating only small dissipation of energy.

Fe_S was frequently encountered for periods when there was no or only small amounts of shedding of wave energy. However, it should be noted that there were several cases of constant E_p versus height when Fe_S were not observed; hence from our data, constant potential energy density versus height is not an indicator of Fe_S presence.

In the mesopause region, gravity waves shed their energy into the surrounding atmosphere through effects such as breaking or overturning (e.g. Fritts and Alexander, 2003). When this happens the potential energy associated with overall gravity wave activity decreases with altitude in this region. However, the solid line in Fig. 9 indicates that, for the period when Fe_S was observed, no or much less energy transfer from the gravity waves to the atmosphere occurred at heights of the sporadic layers. Hence, breaking gravity waves, which lead to a mixing of the atmosphere, could be related to the destruction of Fe_S. As Kane and Gardner (1993) have linked sporadic E layers to Fe_S and as sporadic E can be formed by AGW-induced wind shear, it is possible that the gravity wave dynamics could be the causes for both generation and destruction of Fe_S at different time.

5. Conclusion

A total of 296 h of lidar data was collected at Rothera during 2003, which included 42.3 hours of Fe_S with an overall occurrence probability of 14%. Strong diurnal and semidiurnal tidal modulation of occurrence probability was observed at Rothera, with maximum of 28% at 15:00 LT and zero between 05:00 and 11:00 LT, based on a harmonic fit to the measurements. The occurrence probability of Fe_S exhibits seasonal variations with a maximum of 18% during summer and a minimum of 2% during winter, however, this could be influenced by predominantly summer-daytime and winter-nighttime observations. It was also found that the mean height of Fe_S changed through the year. The fitted altitudes values range from 103 km in the summer to 90 km during the winter period. However, no significant variation in layer width was observed. We investigated potential energy dissipation during and after the occurrence of Fe_S. It was found that in the majority of cases the potential energy density grew conservatively with increasing height when Fe_S was present. Whereas when there was no Fe_S the potential energy decreased with height due to shedding of AGW energy. It is suggested that the energy transfer of shedding AGW enhances the destruction of the sporadic iron layer. Additionally we observed that during sporadic iron layer events the ambient temperature was increased by an average of 20 K.

Acknowledgements

The operation of all instruments at Rothera station is supported by the UK Natural Environment Research Council. In addition, the Fe Boltzmann lidar was supported by Unites States of America National Science Foundation (NSF) grants ATM-03-034357.

The authors are very grateful to the anonymous reviewer and to Dr. Jeffrey Thayer, Editor, for their useful comments in improving the earlier version

References

Alpers, M.J., Blix, T., Kirkwood, S., Krankowsky, D., Lübken, F.-J., Lutz, S., von Zahn, U., 1993. First simultaneous measurements of neutral and ionized iron densities in the upper mesosphere. Journal of Geophysical Research 98 (A1), 275–283.

Alpers, M., Hoeffner, J., von Zahn, U., 1994. Sporadic Fe and E layers at polar, middle and low latitudes. Journal of Geophysical Research 99 (A8), 14971–14985.

Beatty, T.J., Collins, R.L., Gardner, C.S., 1989. Simultaneous radar and lidar observations of sporadic E and Na layers at Arecibo. Geophysical Research Letters 16 (9), 1019–1022.

Clemesha, B.R., Kirchhoff, V.W.J.H., Simonich, D.M., Takahashi, H., 1978. Evidence of an extra-terrestrial source for the mesospheric sodium layer. Geophysical Research Letters 5 (10), 873–876.

Chu, Z., Pan, W., Papen, G., Gardner, C.S., Gelbwachs, J., 2002. Fe Boltzmann temperature lidar: design, error analysis, and initial results at the North and South Poles. Applied Optics 41, 4400–4410.

Cox, R.M., Plane, J.M.C., 1998. An ion-molecule mechanism for the formation of neutral sporadic Na layers. Journal of Geophysical Research 103 (D6), 6349–6359.

Espy, P.J., Hibbins, R.E., Jones, G.O.L., Riggin, D.M., Fritts, D.C., 2003. Rapid, large-scale temperature changes in the polar mesosphere and their relationship to meridional flows. Geophysical Research Letters 30 (5), 1240.

Friedman, J.S., González, S.A., Tepley, C.A., Zhou, Q., Sulzer, M.P., Collins, S.C., Grime, B.W., 2000. Simultaneous atomic and ion layer enhancements observed in the mesopause region over Arecibo during the Coqui II sounding rocket campaign. Geophysical Research Letters 27 (4), 449–452 1999GL900605.

Fritts, D.C., Alexander, M.J., 2003. Gravity wave dynamics and effects in the middle atmosphere. Review of Geophysics 41 (1), 1003.

Gardner, C.S., Kane, T.J., Hecht, J.H., Walterscheid, R.L., Yee, J.H., Niciejewski, R.J., Lowe, R.P., Turnbull, D.N., 1991. Formation characteristics of sporadic Na layers observed simultaneously by lidar and airglow instruments during ALOHA-90. Geophysical Research. Letters 18 (7), 1369–1372.

Gardner, C.S., Kane, T.J., Senft, D.C., Qian, J., Papen, G.C., 1993. Simultaneous observations of sporadic E, Na, Fe, and Ca^+ layers at Urbana, Illinois: three case studies. Journal of Geophysical Research 98 (D9), 16865–16873.

Gardner, C.S., Tao, X., Papen, G.C., 1995. Observations of strong wind shears and temperature enhancements during several sporadic Na layer events above Haleakala. Geophysical Research Letters 22 (20), 2809–2812.

Granier, C., Jegou, J.P., Megie, G., 1989. Iron atoms and metallic species in the earth's upper atmosphere. Geophysical Research Letters 16 (3), 243–246.

Hagan, M.E., Forbes, J.M., 2003. Migrating and nonmigrating semidiurnal tides in the upper atmosphere excited by tropospheric latent heat release. Journal of Geophysical Research 108 (A2), 1062.

Hansen, G., von Zahn, U., 1990. Sudden sodium layers in polar latitudes. Journal of Atmospheric and Terrestrial Physics 52 (6-8), 585–608.

Hauchecorne, A., Chanin, M.-L., 1980. Density and temperature profiles obtained by lidar between 35 and 70 km,. Geophysical Research Letters 7 (8), 565–568.

Helmer, M., Plane, J.M.C., 1990. A model of meteoric iron in the upper atmosphere. Journal of Geophysical Research 103 (D9), 10913–10925.

Kane, T.J., Gardner, C.S., 1993. Structure and seasonal variability of the night time mesospheric Fe layer at midlatitudes. Journal of Geophysical Research 98 (D9), 16875–16886.

Kirchhoff, V.W.J.H., Clemesha, B.R., 1973. Atmospheric sodium measurements at 23°S. Journal of Atmospheric and Terrestrial Physics 35, 1493–1498.

Nagasawa, C., Abo, M., 1995. Lidar observations of a lot of sporadic sodium layers in mid-latitude. Geophysical Research Letters 22 (3), 263–266.

Pan, W., Gardner, S.S., 2003. Seasonal variations of the atmospheric temperature structure at South Pole. Journal of Geophysical Research 108 (D18), 4564.

Pendleton Jr., W.R., Espy, P.J., Hammond, M.R., 1993. Evidence for non-local-thermodynamic-equilibrium rotation in the OH nightglow. Journal of Geophysical Research 198 (A7), 11567–11579.

Picone, J.M., Hedin, A.E., Drob, D.P., Aikin, A.C., 2002. NRLMSISE-00 empirical model of the atmosphere: statistical comparisons and scientific issues. Journal of Geophysical Research 107 (A12), 1468.

Plane, J.M.C., Murray, B.J., Chu, X., Gardner, C.S., 2003a. Removal of meteoric iron on polar mesospheric clouds. Science 304, 426–428.

Plane, J.M.C., Self, D.E., Vondrak, T., Woodcock, K.R.I., 2003b. Laboratory studies and modeling of mesospheric iron chemistry. Advanced Space Research 32 (5), 699–708.

Qian, J., Gu, Y., Gardner, C.S., 1998. Characteristics of sporadic Na layers observed during the airborne lidar and observations of Hawaiian airglow/airborne noctilucent cloud (ALOHA/ANLC-93) campaigns. Journal of Geophysical Research 103 (D6), 6333–6347.

Siskind, D.E., Eckermann, S.D., McCormack, J.P., Alexander, M.J., Bacmeister, J.T., 2003. Hemispheric differences in the temperature of the summertime stratosphere and mesosphere. Journal of Geophysical Research 108 (D2).

von Zahn, U., von der Gathen, P., Hansen, G., 1987. Forced release of sodium from upper atmospheric dust particles. Geophysical Research Letters 14 (1), 76–79.

Whiteway, J.A., Carswell, A.I., 1994. Rayleigh lidar observations of thermal structure and gravity wave activity in the High Arctic during a stratospheric warming. Journal of Atmospheric Science 51 (2), 3122–3136.